Proceedings of the Research Institute of Atmospherics,
Nagoya University, vol. 19 (1972)

VLF HISS OBSERVED AT SYOWA STATION, ANTARCTICA-I

Observation of VLF hiss

Yoshihito TANAKA

Abstract

VLF hiss observed at Syowa Station may be divided into steady and impulsive types. The steady VLF hiss which appears in association with moderate geomagnetic activity and weak cosmic noise absorption (CNA) at 30 MHz, continues from ten to several tens of minutes and dominates in the lower frequency range (5-12kHz), usually occurring in the evening side of the nighttime. Near the magnetic midnight, an impulsive VLF hiss occurs almost synchronously with the auroral break-up always followed by sharp and large fluctuations of magnetic H-component and CNA. It falls sharply in short period before the maximum activity of the aurora and its frequency range extends more than 100 kHz.

Through a polarimeter, VLF hiss is divided into right-handed polarized (R-) component and left-handed polarized (L-) component. The polarization record teaches us that VLF hiss is right-handed polarized. However, the ratio of R-component to L-component was smaller than we had expected. Supposed that VLF hiss comes down to the ground with nearly circular polarization and small angle of incidence, the polarization data seem to be explained by the simultaneous arrival of multiple rays uncorrelated.

Displaying Lissajous' figures on a cathode ray tube, we investigated the polarization, incident angle and arriving direction of VLF hiss (hereafter the method is called as CRT method). The figures show that VLF hiss propagates downward with not so large an angle of incidence, roughly within the magnetic meridian plane.

1. Introduction

Since Ellis (1959) first observed the continuous type VLF emissions (VLF hiss) with the minimum level reading circuit devised by himself, the observation of VLF

hiss has been advanced. The occurrence of VLF hiss has been actively studied. However, as to the polarization, incident angle and arriving direction of VLF hiss, even the observations have not been enough. Direction finding experiments were carried out with goniometer arrangements (Ellis 1960, Iwai & Tanaka 1968, Vershinin 1970) and by means of alternately switching loop antennas to a preamplifier (Harang & Hauge 1965). The observations on polarization were made with a polarimeter system (Iwai & Tanaka 1968, Tanaka et al. 1970) and by means of displaying polarization patterns on an oscillograph (Harang & Hauge 1965, Nishino & Tanaka 1969, Tanaka et al. 1970).

Since 1967, at Syowa Station (-69.6° geomagnetic latitude) we had been observing the intensity, polarization, incident angle and arriving direction of VLF hiss with the minimum level reading circuit, the polarimeter system and the CRT method.

In part I of this paper, we will introduce the observing method adopted and explain the principle of the observation. Then, we will show some obtained data and outline general features of VLF hiss in the auroral zone (auroral hiss). Moreover, we will discuss the interference from atmospherics and artificial noises, and the problems arising due to multiple rays and low ground conductivity.

The purpose of part II is to make statistical investigations into the occurrence and polarization of VLF hiss events and to clarify some characteristics on the propagation of auroral hiss.

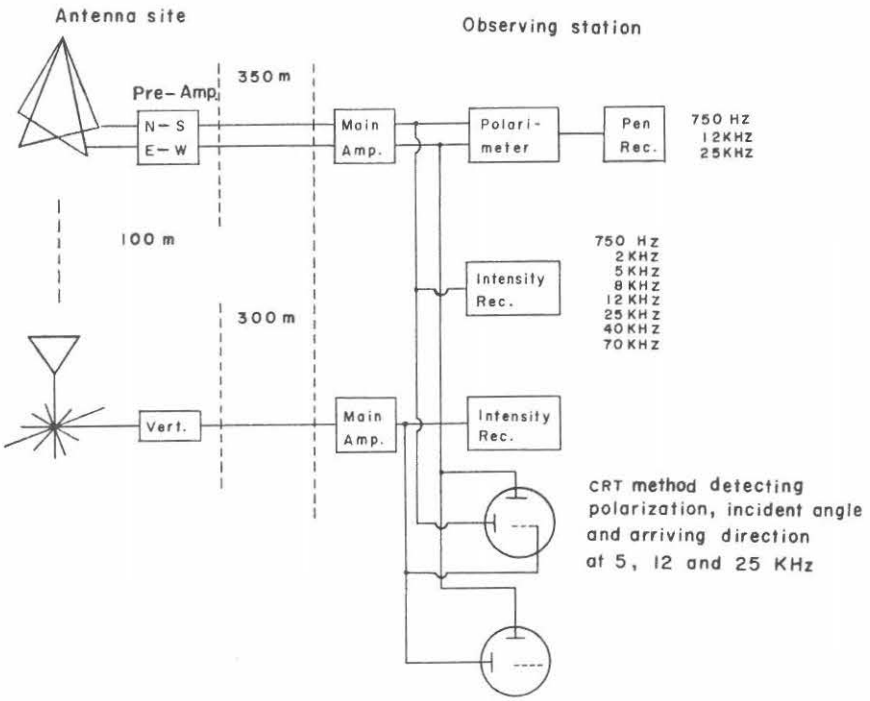

Fig. 1. Block diagram of the apparatus at Syowa Station in 1968.

2. Observing technique

Fig. 1 shows the block diagram of the apparatus at Syowa Station. The antenna system consists of a pair of crossed loops directed in geographical N-S and E-W and a vertical antenna. The loop antenna is of the triangle type of two turns and its dimension is 20 m in height and 40 m at the base. The vertical antenna is a pipe of 10 m long. In order to reduce the interfering disturbances induced for very low conductivity of the ground, the counterpoise is set radially with 35 copper wires of 15 m long around the vertical antenna. The preamplifiers are installed just under the antennas and each of the output signals is led by a twin-ax cable of 300-350 m long to the main amplifier in the observation room. The signals through the main amplifiers are supplied to the intensity meter, the polarimeters and the cathode ray tubes, respectively.

2-1 Observation of intensity

The intensity meter consists of narrow band amplifiers and pen-oscillographs. In the narrow band amplifiers, the signals (N-S signals as are generally used) are selected in eight ranges of center frequencies at 0.75, 2, 5, 8, 12, 25, 40 and 70 kHz by band pass filters ($Q=10$) and each signal selected is rectified to d-c and averaged for 10 milli-seconds and then fed to the resistance-capacitance circuit with a charging time constant of 5 seconds and a discharging time constant of 2 milli-seconds. The d-c output is recorded on a chart paper moving at 10 cm/hour.

2-2 Observation of polarization with polarimeter and pen-oscillograph method

Fig. 2 shows the block diagram of polarimeter and pen-oscillograph system. A polarimeter is composed of one pair of phase shifters and two band pass amplifiers. Through a pair of phase shifters, either N-S or E-W signal is led and lagged in phase by right angle at the frequency selected by the following band pass filter and added to the other signal. Then, the incoming signals are divided into right-handed polarized component and left-handed polarized component. The divided signals are respectively introduced to the band pass amplifiers with band pass filters of center frequencies at 0.75, 12 and 25 kHz and of which $Q=40$. Then, each signal is supplied to the detecting circuit with the same property as the intensity meter's and the output is recorded on a chart paper moving at 10 cm/hour.

2-3 *Observation of polarization, incident angle and arriving direction with CRT method*

Fig. 3 shows the block diagram of CRT method detecting polarization, incident angle and arriving direction at 5, 12 and 25 kHz. The signals of N-S and E-W channels are given to a goniometer and then supplied to band pass amplifiers in which phase and gain adjustments are strictly made to eliminate the differences of phase and gain induced in the two receiving systems. When a vertical signal is given to a CRT, its phase shift caused in the all receiving system, involving the antenna must be equal to N-S and E-W signals'. So, the phase of the vertical signal is adjusted in the phase shifter. These phase adjustments of the receiving systems are made by giving test signals to dummy antenna circuits installed instead of observing antennas.

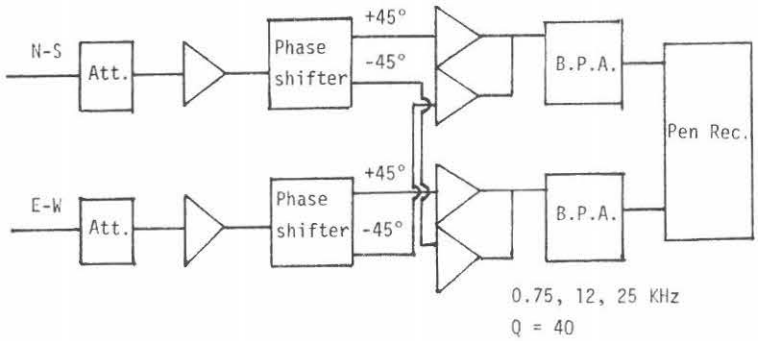

Fig. 2. Black diagram of polarimeter and pen-oscillograph system.

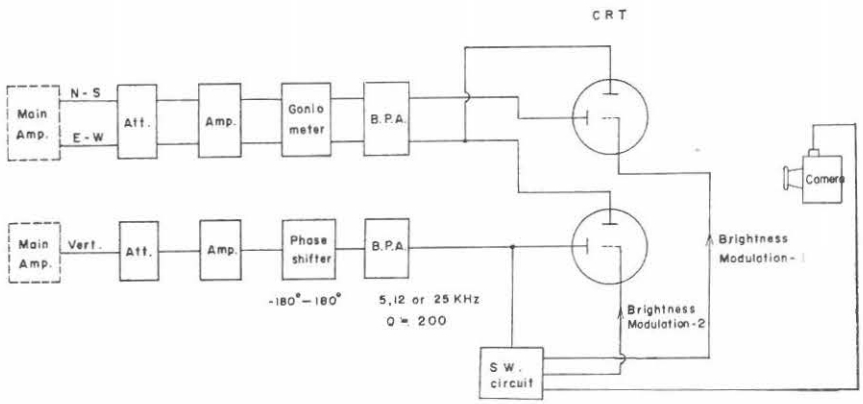

Fig. 3. Block diagram of CRT method detecting polarization, incident angle and arriving direction at 5, 12 and 25 kHz.

The outputs from N-S and E-W channel band pass amplifiers (B. P. A., Q=200) are introduced to a CRT. One of these outputs and an output from the vertical channel B. P. A. (Q=200) are given to the other CRT. The other output from the vertical channel B. P. A. is supplied to the switching circuit, from which two output signals modulate the brightnesses of the pictures on the two cathode ray tubes, respectively.

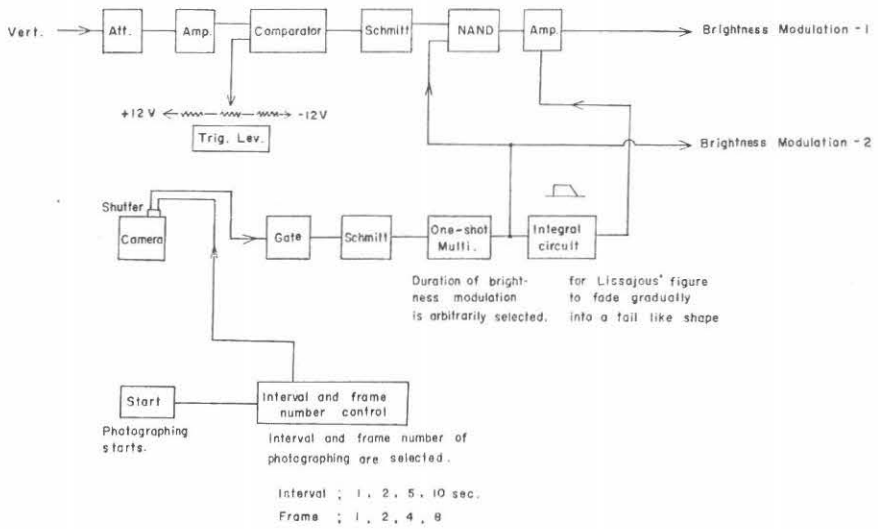

Fig. 4. Block diagram of switching circuit.

Fig. 4 shows the block diagram of the switching circuit. When a signal of photographing start is given, the interval (1, 2, 5 or 10 seconds) and frame number (1, 2, 4 or 8) of photographing are selected in the interval and frame number control circuit. On the other hand, the starting signal pushes the shutter of the camera. A gate signal which synchronizes with the shutter's movement is shaped and then supplied to an one-shot multivibrator in which the duration of brightness modulation is arbitrarily chosen. The output from the one-shot multivibrator is modified in the integral circuit so that a Lissajous' figure fades gradually into a tail like shape. As the result, the sense of rotation of the magnetic field can be easily known. Only when the amplitude of the vertical signal is greater than or equal to zero level, the picture described by the N-S and E-W signals is desired to be displayed on a CRT. So, d-c bias is added so that the Schmitt triggering starts at the zero level of the vertical signal. Then, the output from the Schmitt circuit is modified by the outputs from the one-shot multivibrator and the integral circuit. And the modified signal is added to the cathode of a CRT so that the brightness modulation begins at the zero level

of the vertical signal and continues only during plus half cycles.

At the station where the sources of VLF hisses are just over the observing point and where some waves with not so large incident angles are received at the same time, it is generally difficult to use a goniometer arrangement. For our practical observation, a goniometer arrangement was non-effective, so that the goniometer remained fixed. The figure described by N-S and E-W signals is, in practice, displayed only during a few plus half cycles of the vertical signal. Then, two CRT patterns are simultaneously photographed and all physical properties of VLF hiss are analysed with the photograph.

3. Principle of the observation

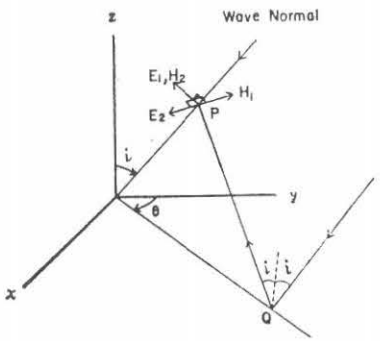

Fig. 5. Coordinate system.

The principle of the observational method of atmospherics was once discussed by Iwai (1962) and this could be applied for the Antarctic observation. The symbols used are listed below.

x, y, z : cartesian coordinate ; z is measured vertically upward, y is directed toward geographical north and x-y plan is the ground.

w : angular wave frequency ; a time factor exp (jwt) is used in this paper.

i : incident angle

θ : azimuthal angle

H_x, H_y, H_z : x, y and z components of magnetic field at a point P

E_x, E_y, E_z : x, y and z components of electric field at a point P

E_1, H_1 : electric and magnetic components of TM mode wave

E_2, H_2 : electric and magnetic components of TE mode wave

ρ_1, ρ_2 : complex reflection coefficients of TM and TE mode waves

A_1; A_2 : amplitudes of magnetic fields of TM and TE mode waves

λ : wave length

ϕ : phase difference between TM and TE mode wave

h : height of a receiving point P

Each component of magnetic and electric fields at P is

$$H_x = \left\{-1+\rho_2 \exp\left(-j\frac{4\pi h}{\lambda}\cos i\right)\right\} H_2 \cos i \cdot \sin\theta - \left\{1+\rho_1 \exp\left(-j\frac{4\pi h}{\lambda}\cos i\right)\right\} H_1 \cos\theta$$

$$H_y = \left\{-1+\rho_2 \exp\left(-j\frac{4\pi h}{\lambda}\cos i\right)\right\} H_2 \cos i \cdot \cos\theta + \left\{1+\rho_1 \exp\left(-j\frac{4\pi h}{\lambda}\cos i\right)\right\} H_1 \sin\theta$$

$$H_z = \left\{1+\rho_2 \exp\left(-j\frac{4\pi h}{\lambda}\cos i\right)\right\} H_2 \sin i$$

$$E_x = \left\{-1+\rho_1 \exp\left(-j\frac{4\pi h}{\lambda}\cos i\right)\right\} E_1 \cos i \cdot \sin\theta + \left\{1+\rho_2 \exp\left(-j\frac{4\pi h}{\lambda}\cos i\right)\right\} E_2 \cos\theta$$

$$E_y = \left\{-1+\rho_1 \exp\left(-j\frac{4\pi h}{\lambda}\cos i\right)\right\} E_1 \cos i \cdot \cos\theta - \left\{1+\rho_2 \exp\left(-j\frac{4\pi h}{\lambda}\cos i\right)\right\} E_2 \sin\theta$$

$$E_z = \left\{1+\rho_1 \exp\left(-j\frac{4\pi h}{\lambda}\cos i\right)\right\} E_1 \sin i$$

Here, we assume as follows.

(a) VLF hiss, in general, a downcoming plane wave and is elliptically polarized.

(b) The ground is flat and perfectly conductive.

(c) The wave is a monochromatic sine wave.

The assumption (a) is, perhaps, reasonable for the reception of the VLF hiss within a source area. It is possible in most cases to assume that the ground is perfectly conductive for VLF range. The assumption (c) may be accepted if the narrow band pass filters are used and the patterns for the initial and a few more cycles are discussed.

Thus, we assume $\rho_1 = 1$, $\rho_2 = -1$ and $\lambda \gg h$

hence,

$$H_x = -2A_2 \cos i \cdot \sin\theta \cdot \sin(wt+\phi) - 2A_1 \cos\theta \cdot \sin wt$$

$$H_y = -2A_2 \cos i \cdot \cos\theta \cdot \sin(wt+\phi) + 2A_1 \sin\theta \cdot \sin wt$$

$$E_z = 2A_1 \sin i \cdot \sin wt$$

$$H_z = E_x = E_y = 0$$

where,

$$H_1 = A_1 \sin wt$$

$$H_2 = A_2 \sin(wt+\phi)$$

$$E_1 = A_1 \sin wt$$

It is, therefore, clear that only H_x, H_y and E_z have to be discussed for VLF range.

3-1 Observation of polarization with polarimeter and pen-oscillograph method

Through a phase shifting circuit, H_x component is led and lagged in phase by right angle and each is added to H_y, respectively.
Accordingly,

$$\text{Amplitude of } (H_x^{\pm}+H_y) = 2\{(A_2^2\cos^2 i + A_1^2) \pm 2A_2 A_1 \cos i \cdot \sin\phi\}^{1/2}$$

put

$$C = \frac{\text{amplitude of } (H_x^- + H_y)}{\text{amplitude of } (H_x^+ + H_y)} = \left[\frac{k^2+1-2k\sin\phi}{k^2+1+2k\sin\phi}\right]^{1/2} = R/L \quad \cdots\cdots\cdots (1)$$

where,

H_x^+ : H_x led in phase by 90°

H_x^- : H_x lagged in phase 90°

$k = A_2 \cos i / A_1$

R/L : ratio of R-component to L-component

then,

if $C > 1$: right-handed elliptically polarized

if $C < 1$: left-handed elliptically polarized

if $C = 1$: linearly polarized

Here, the right-handed sense means that the electric and magnetic vectors rotate clockwise when the observer is looking in the direciion of the earth's magnetic field.

The C values for different ϕ's as a parameter of k are shown in Fig. 6.

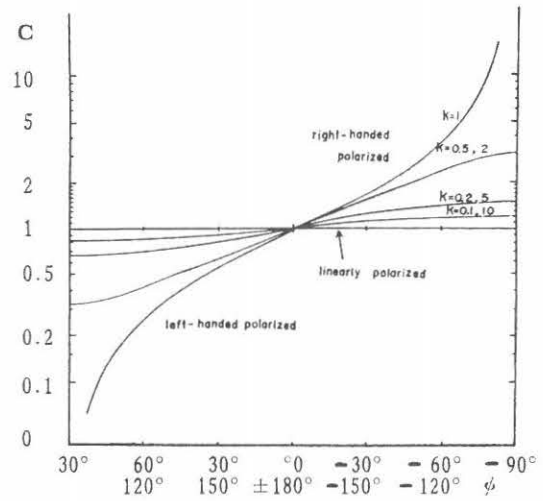

Fig. 6. C values for different ϕ's as a parameter of k.

3-2 Observation with CRT method

Within a source area, it is generally non-effective to use a goniometer arrangement. Hence, we explain in this section the observing method with fixed crossed loops. So, H_x-H_y figure displaying only during plus half cycles of E_z (Fig. 7-1), and H_x-E_z figure (Fig. 7-2) are used to find the physical quantities of VLF hiss. If $E_z = 0$, $H_x/H_y = \tan\theta$ for the cutting axis of the half ellipse. Thus, the symmetric line for the cutting axis with respect to the straight line $H_x = H_y$ gives the arriving direction. And the direction is determined without 180° ambiguity, through a simple analysis. If the coordinate axes are rotated counter-clockwise by angle θ and the new axes are written as $\overline{H}_x$ & $\overline{H}_y$, then $\overline{H}_x$ & $\overline{H}_y$ can be given as follows.

$$\overline{H}_x = -2A_1 \sin wt, \qquad \overline{H}_y = -2A_2 \sin(wt+\phi)\cos i$$

This is the same expression as H_x, H_y when $\theta = 0°$.

So, we can get $A_2 \cos i/A_1$ and $|\sin\phi|$, as shown in Fig. 8 and then ϕ can be obtained in a simple analysis. H_x-E_z figure is an ellipse in general and in this figure we get $m/p = \sin i / (k \mid \sin\theta \cdot \sin\phi \mid)$, from which we can determine i value. Thus, all quantities can be obtained without any ambiguity.

The above-mentioned treatment is for a single wave and moreover the above discussion is reasonable only when the intensity of one wave is much more dominant than those of the other waves, even if some signals are simultaneously received from multi-directions within a source area.

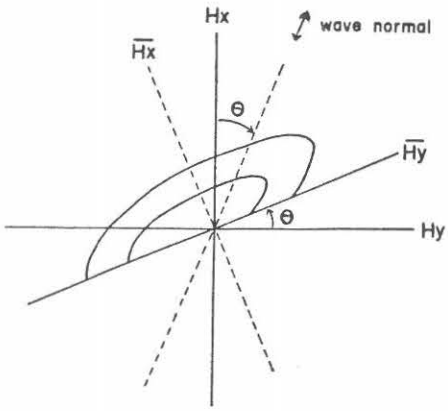

H_x-H_y, the figure during plus half cycle of E_z.

Fig. 7-1

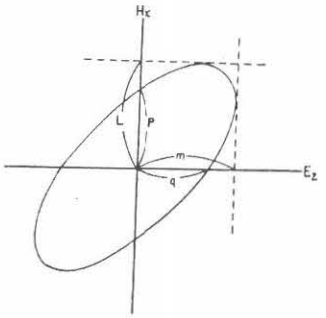

H_z-E_z pattern

Fig. 7-2

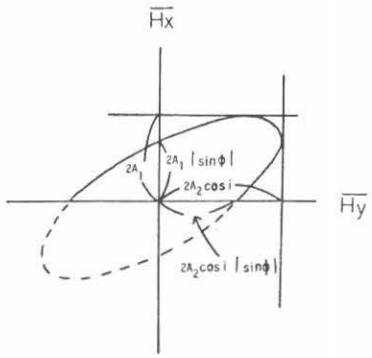

Fig. 8. $\overline{H}_x - \overline{H}_y$ pattern.

4. Observed results

4-1 General features of VLF hiss

Fig. 9 shows the diurnal and seasonal variation of the occurrence of VLF hiss at 12 kHz. The occurrences in the other frequencies (2, 5, 8 and 25 kHz) also have been found to be of the same tendency (not shown in this paper). It is seen in the figure that the activity is the greatest before the magnetic midnight and the occurrences concentrate in the local night and that the occurrences are limited in winter

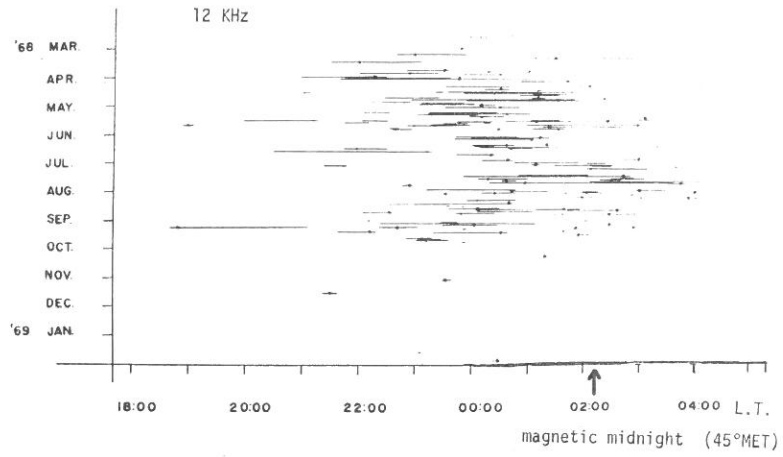

Fig. 9. Diurnal and seasonal variation of the occurrences of VLF hisses at Syowa Station; A dot represents the peak of an event.

and at equinoxes and are very few in summer. The decrease of the occurrences in summer is thought to be caused by the ionospheric absorption.

General aspects of the VLF hiss observed at Syowa Station are typically shown in figures 11-18 which represent VLF hiss events, their polarizations, geomagnetic H-components and cosmic noise absorptions (CNA) at 30 MHz. The steady VLF hiss which appears in association with moderate geomagnetic activity and weak CNA, continues from ten to several tens of minutes and dominates in the lower frequency range (5-12 kHz) and usually occurs in the evening side of the nighttime, as shown in figures 12, 16, 17 and 18.

Near the magnetic midnight, an aurora breaks up around the zenith and the auroral break-up is always followed by sharp and large fluctuations of magnetic H-component and CNA. There appears to be usually a time delay of a few minutes between the outburst of aurora and the increase in CNA (Holt & Omholt 1962). An impulsive VLF hiss occurs almost simultaneously with the auroral break-up and falls sharply in short period (about several minutes) before the maximum activity of the aurora and its frequency range extends, as shown in figures 13, 14 and 15. Even when an auroral break-up does not occur or can not be observed, an impulsive VLF hiss with a wide band frequency range appears just before the large decrease of geomagnetic H-component, as shown in figures 11. 12, 14, 17 and 18.

The geomagnetic perturbation and the fluctuation of CNA during a polar substorm are thought to be caused by the precipitation of auroral particles into the ionosphere and so they are apparently in phase. On the other hand, VLF hiss has a positive correlation to the weak CNA as shown in Fig. 10. This result coincides with that obtained by Harang & Larsen (1965) at Tromsö (67° geomag. lat.). Whereas, cosmic

radio noise at 30 MHz was recorded at Syowa Station by a standard riometer connected to a vertically direct, five-element Yagi antenna, so that the directivity of the antenna is fairly sharp toward the vertical direction. Moreover, it is not always easy to distinguish in practice a small absorption dip in the riometer datum. So, CNA data are thought to be not more sensitive than geomagnetic data in order to investigate the correlations to VLF hiss events, as found in figures 17 and 18.

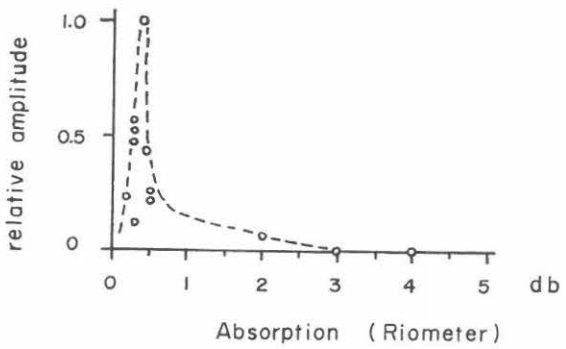

Fig. 10. VLF events at 12 kHz appearing during small absorption dips on the riometer.

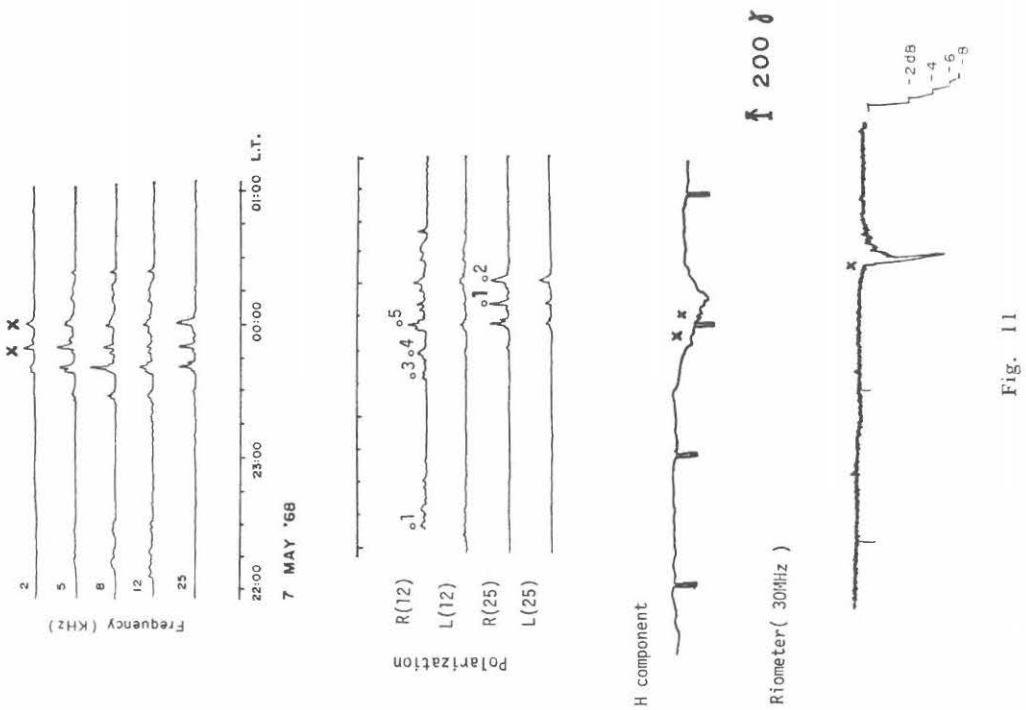

Fig. 11

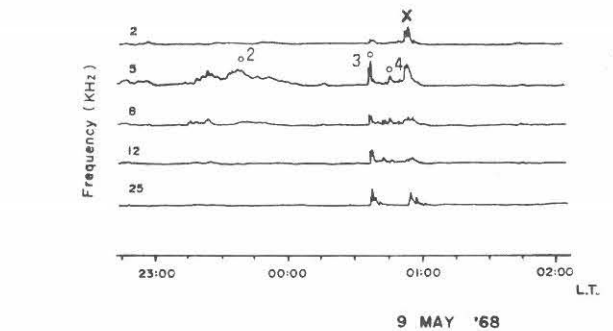
2
5
8
12
25
Frequency (KHz)
23:00
00:00
01:00
02:00
L.T.
9 MAY '68
R(12)
L(12)
R(25)
L(25)
H component
Riometer

Fig. 12

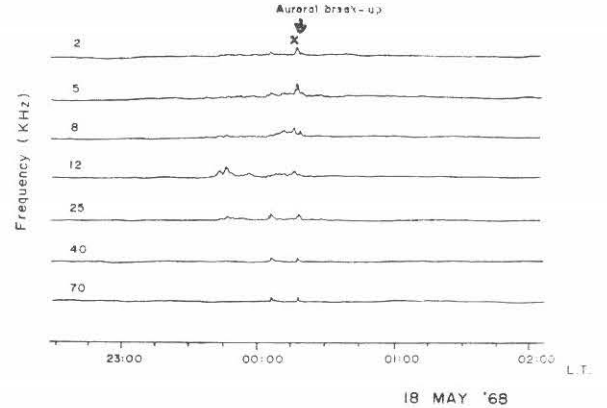
Auroral break-up
2
5
8
12
25
40
70
Frequency (KHz)
23:00
00:00
01:00
02:00
L.T.
18 MAY '68
R(12)
L(12)
R(25)
L(25)
H component
Riometer

Fig. 13

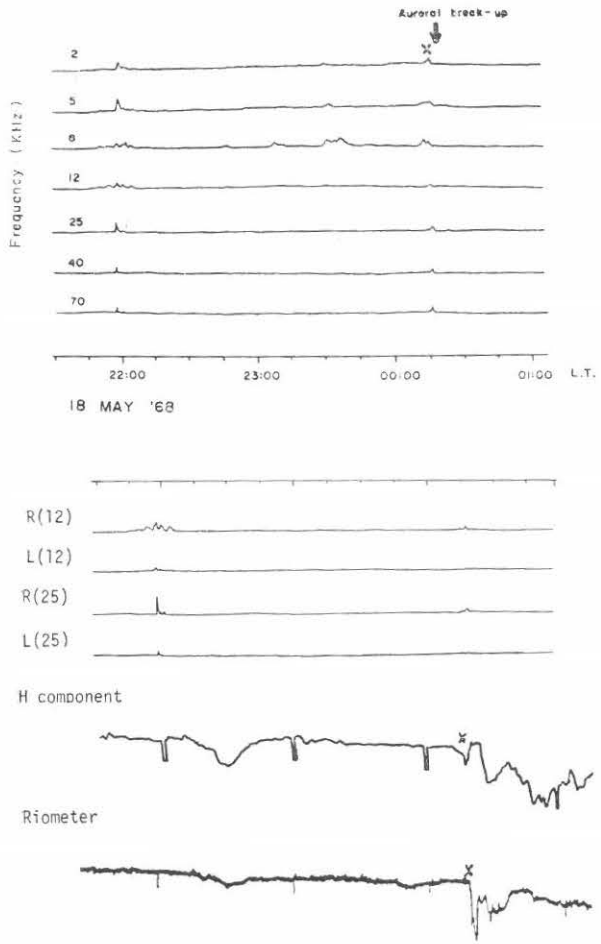
Auroral break-up
2
5
6
12
25
40
70
Frequency (KHz)
22:00
23:00
00:00
01:00
L.T.
18 MAY '68
R(12)
L(12)
R(25)
L(25)
H component
Riometer

Fig. 14

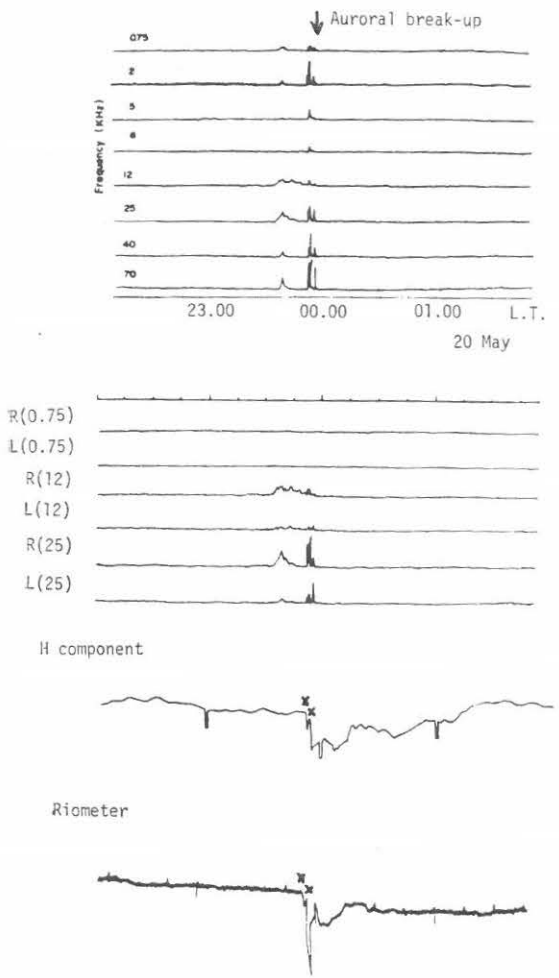
Auroral break-up
0.75
2
5
6
12
25
40
70
Frequency (KHz)
23.00
00.00
01.00
L.T.
20 May
R(0.75)
L(0.75)
R(12)
L(12)
R(25)
L(25)
H component
Riometer

Fig. 15

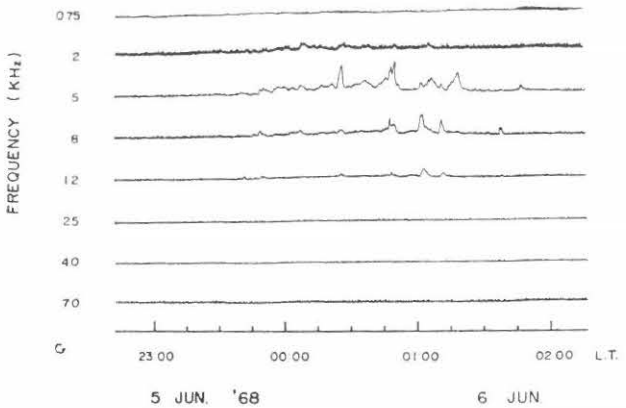

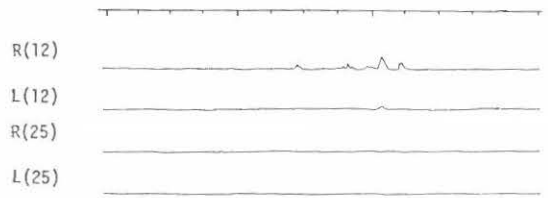

H component

Riometer

Fig. 16

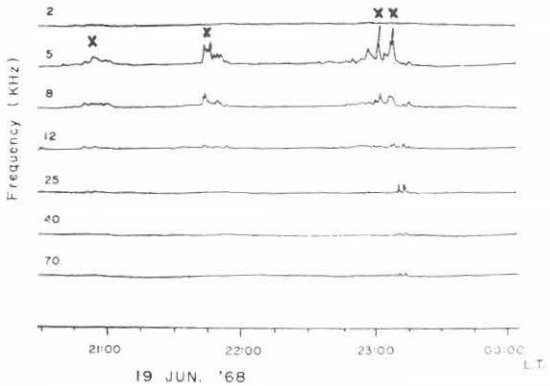

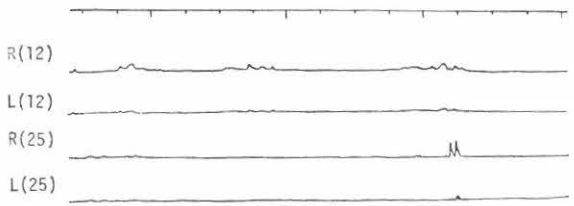

H component

Riometer

Fig. 17

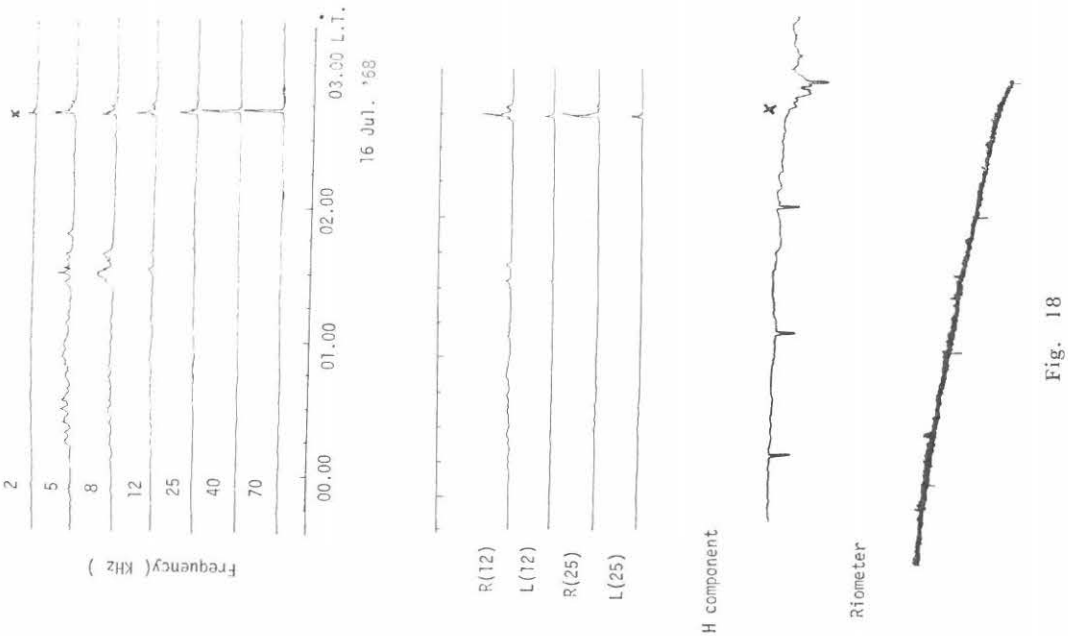

Fig. 18

4-2 Polarization with polarimeter and pen-oscillograph method

Through a polarimeter, VLF hiss is divided into R-component and L-component and the two components are recorded on a chart paper. Fig. 19 represents the ratios of R-components to L-components on the peak levels of VLF hisses at 12 and 25 kHz. In the figure, VLF hisses are shown to be right-handed polarized. However, it is not clear whether VLF hisses are elliptically polarized or they come down with right-handed circular polarization and considerably large incident angles.

On the other hand, it has been supposed that VLF hiss comes down almost vertically along the line of force of the earth's magnetic field in whistler mode (Harang & Hauge, 1965). However, the results shown in Fig. 19 can not be reasonably explained on the assumption that a single wave with circular polarization and with not so large an incident angle is received. Therefore, it is, firstly, necessary to know the polarization of VLF hiss in the free space and secondly to discuss the waves from multi-directions. The problems will be discussed in part II of this paper.

4-3 Polarization, incident angle and arriving direction with CRT method

The observation with the CRT method is very delicate and difficult because of

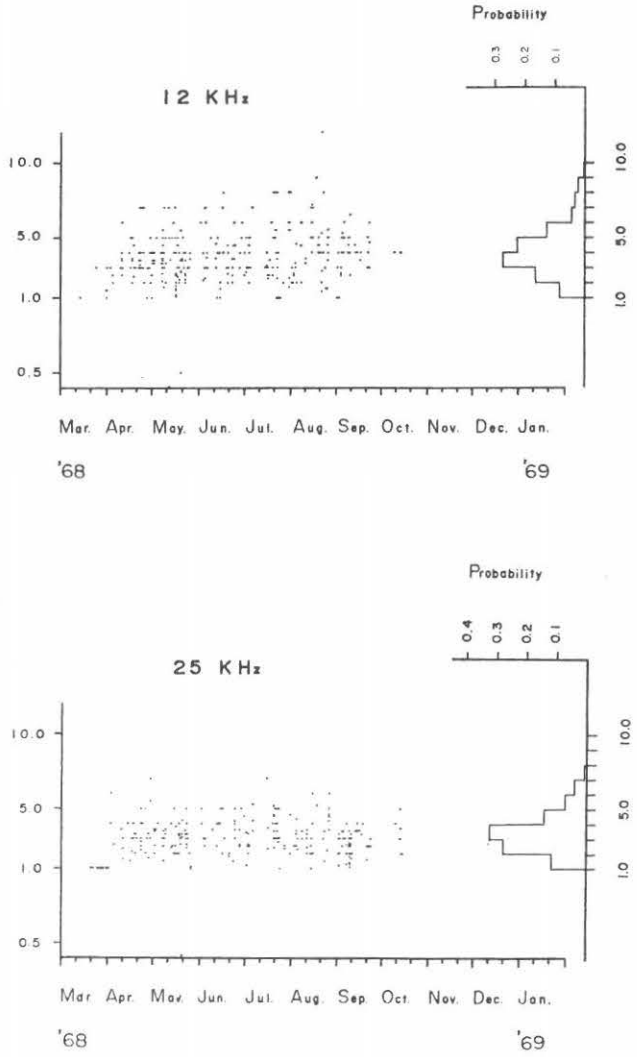

Fig. 19. Ratio of R-component to L-component of VLF hiss.

the technical problem involved in the observational timing and in the separation of the hiss from unwanted atmospherics. So, the number of desirable data is, unfortunately, not so many.

Fig. 20 gives polarizations, incident angles and arriving directions obtained with the CRT method at the VLF events shown in figures 11 and 12. It is found in Fig. 20 that the waves come down to the ground with not so large incident angles and that the arriving directions are nearly parallel to the magnetic meridian plane passing through Syowa Station. Fig. 21 shows some examples of oscillographic patterns.

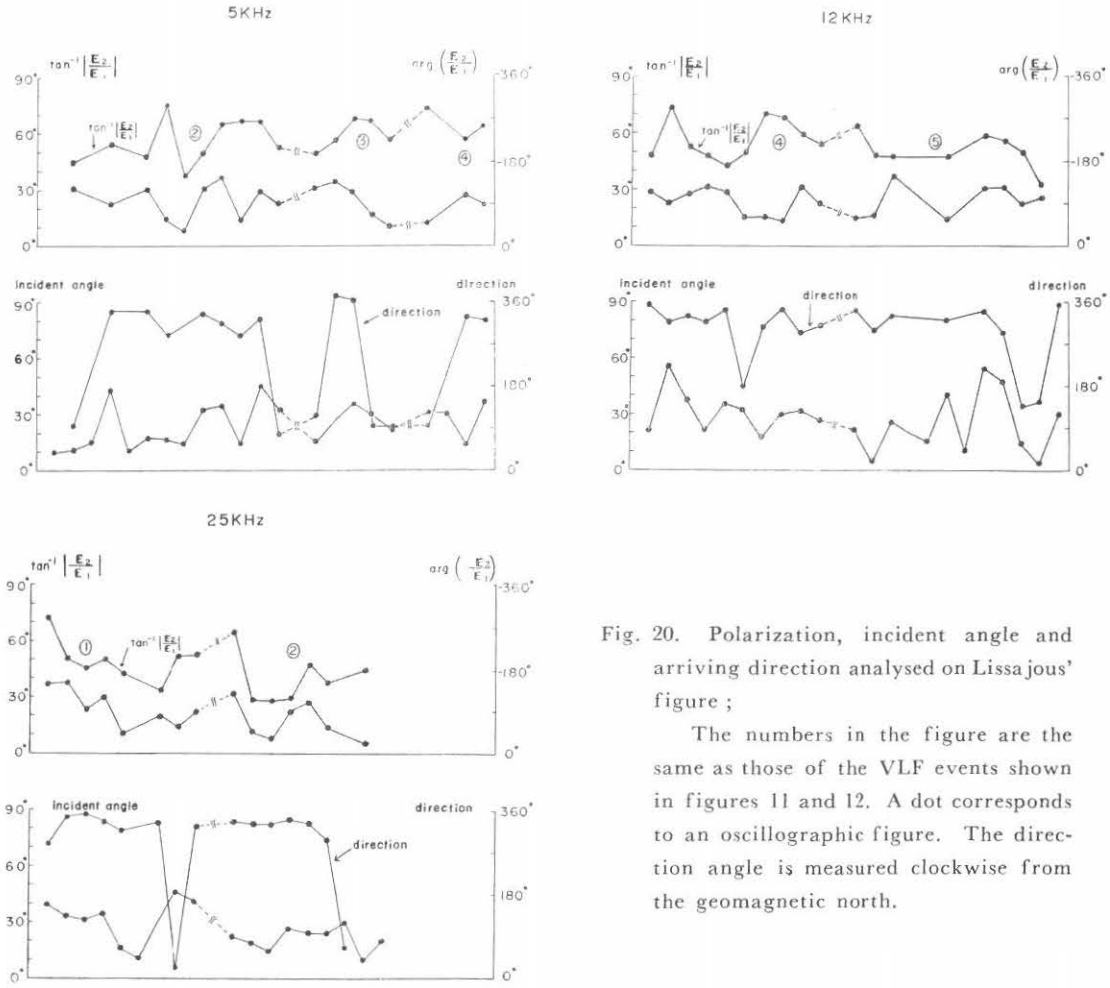

Fig. 20. Polarization, incident angle and arriving direction analysed on Lissajous' figure ;

The numbers in the figure are the same as those of the VLF events shown in figures 11 and 12. A dot corresponds to an oscillographic figure. The direction angle is measured clockwise from the geomagnetic north.

arditrary unit

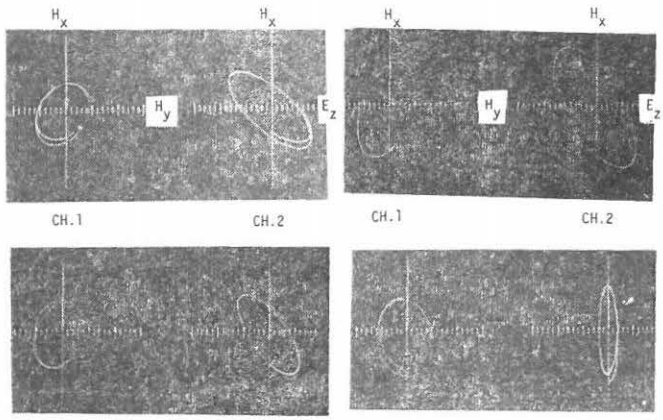

23.40 7 May L. T. 12 kHz.

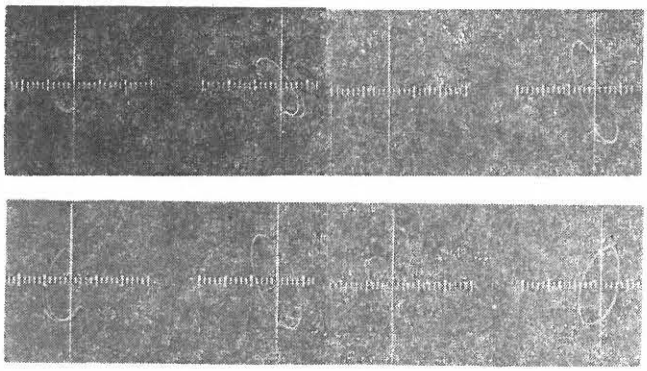

23.50 7 May L. T. 25 kHz.

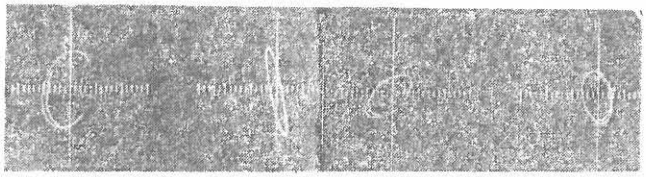

23.29 7 May L. T. 12 kHz.

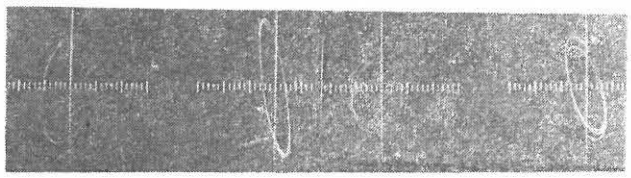

00.02 8 May L. T. 25 kHz.

Fig. 21. Oscillographic patterns: H_x is the geographic east component of magnetic field, H_y is the north component and E_z is the vertical component of electric field.

5. Discussion

5-1 Interference from atmospherics and artificial noises

Even at high latitude, levels of atmospherics are high enough. At Syowa Station, average levels of atmospherics at night in winter are comparable to peak levels of

VLF events. So, a routine and quantitative observation of the intensity is carried out with the minimum level reading circuit developed by Ellis (1959) and Iwai (1964). The circuit is designed in order to be sensitive to continuous signals such as VLF hisses but not sensitive to impulsive noises such as atmospherics. It is composed of the resistance-capacitance circuit with a large charging time constant and a very small discharging time constant. The charging time constant is chosen in consideration of durations of VLF events and the intensity ratios of VLF events to atmospherics. In our case, the charging time constant was 5 seconds and the discharging time constant was 2 milli-seconds. As a result, the attenuation of atmospherics levels through the circuit was more than 20 dB.

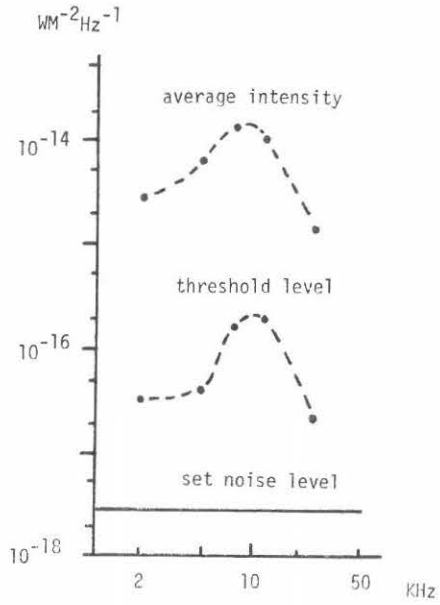

Fig. 22.

For the strict calibration of the intensity and the exact detection of the ratio of R-component to L-component, it is necessary to suppress the noise level induced mainly by atmospherics as low as possible. So, the threshold levels on which VLF events were distinguished, were higher and depended on the receiving frequencies. The intensities in the maximum occurrences of VLF hisses (described as average intensity in Fig. 22) were roughly estimated from Fig. 6 of part II of this paper and they also depended on the frequencies. Both the dependences are nearly similar as shown in Fig. 22. Thus, it is inferred in the figure that the threshold levels were set, as the detections of VLF events were roughly equivalent in the range of the receiving frequency. As the occurrence number of VLF events depends sensitively on the threshold level, it is not reasonable to discuss the absolute value of the occurrence, but it is necessary to pay attention to the relative value and its variation.

At Syowa Station, the ground consists of huge blocks of rocks. So, the ground conductivity is low and the earthing resistance is considerably large. A vertical antenna is unbalanced to the ground. Therefore, artificial noises, power noises in the main, within the station are induced into the top of the apparatus if the earthing resistance is large. We set the counterpoise around the vertical antenna and detected the differential signal of the two outputs from the vertical antenna and the counterpoise in the preamplifier, eliminating the artificial noises and holding the ground to be equivalently perfectly conductive. As a result, the ratios of wanted signals to power noises were improved more than 10 dB.

At Syowa Station, the levels of atmospherics are usually much higher than those of VLF hisses. Moreover, atmospherics propagate almost horizontally, but VLF hisses come down with not so large angles of incidence. Thus, the difference of the two levels comes to be so much larger for the reception of VLF signals with a vertical antenna. Hereby, atmospherics interfere very often especially in the vertical signals. Then, it is considerably difficult to obtain desirable Lissajous' figures in the observation with the CRT method.

5-2 Multiple rays

In this section, we will discuss the following problem. How fairly do the physical properties obtained for a single wave on a Lissajous' figure describe those of individual waves if the received signal is composed of multiple waves ?

It has been supposed that VLF hiss came down vertically along the field line with right-handed circular polarization. We will suggest in part II that VLF hiss comes down to the ground with right-handed circular polarization and not so large an incident angle, roughly within the magnetic meridian plane, and that multiple waves downcoming with different incident angles and independent phases are usually simultaneously received.

For a simple example, we will take up two waves coming down from the geomagnetic north with equal amplitude, right-handed circular polarization and incident angles of 30°, 50°. Fig. 23 shows CRT patterns described when the two waves are simultaneously received and the phase difference (α) changes. Whereas, physical properties given in the figure is obtained on the assumption that a single wave is received.

In the figure, it is found that the physical properties analysed on oscillographic patterns are remarkably different from those of each wave. However, the properties roughly speaking may be supposed to show those of each wave or the average values, if the phese difference is not so large. Usable oscillographic patterns in the analysis are very few chiefly because of the interference from atmospherics and multiple rays. But these usable patterns are supposed to satisfy the condition that phase differences are not so large. Therefore, when multiple rays are received at the same time, it is unable to find precisely the physical properties of individual waves but it is able to investigate the average values of the properties in the observation with the CRT method.

In few cases of isolated and sharp VLF bursts, the CRT method is of course effective.

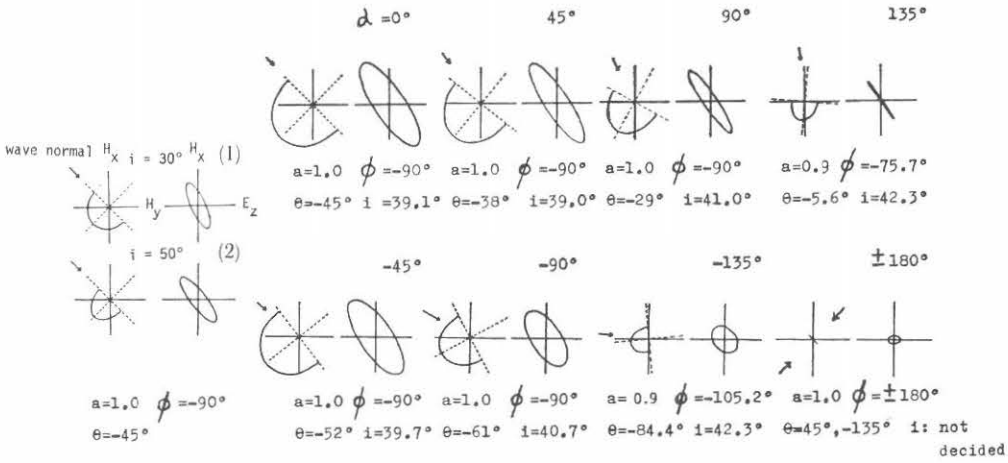

Fig. 23. Lissajous' figures on CRT and physical properties obtained in the time when two waves are received at the same time with right-handed circular polarization, equal intensity, azimuthal angle of -45° (geomagnetic north) and incident angles of 30°, 50° and the phase difference (α) changes. (α) is given by $wt_2 = wt_1 + \alpha$. (1) is to the wave with incident angle of 30° and (2) is to the wave with incident angle of 50°. An arrow shows a wave normal directoin. "a" represents (A_2/A_1).

5-3 *Errors due to low ground conductivity*

When the ground conductivity is low, a Lissajous' figure is usually different from that for perfect conductivity. Hence, the physical quantities obtained in the figure on the assumption that the ground is perfectly conductive, are thought to be generally not true. Moreover, a polarization obtained with the polarimeter and pen-oscillograph system is also thought to be affected.

The reflection coefficient ρ_1 and ρ_2 are complex in general and written as follows.

$$\rho_1 = \frac{N^2 \cos i - (N^2 - \sin^2 i)^{1/2}}{N^2 \cos i + (N^2 - \sin^2 i)^{1/2}} = |\rho_1| \exp(-j\Theta_1)$$

$$\rho_2 = \frac{\cos i - (N^2 - \sin^2 i)^{1/2}}{\cos i + (N^2 - \sin^2 i)^{1/2}} = |\rho_2| \exp(-j\Theta_2)$$

$$N^2 = \kappa - j(\sigma/2\pi f \varepsilon_0)$$

where, N : refractive index of the ground
σ : specific conductivity
$\kappa = \varepsilon/\varepsilon_0$: dielectric constant (specific inductive capacity)
ε_0 : dielectric constant of free space

Then, each component of magnetic and electric fields at a receiving point is

$$\left.\begin{aligned} H_x &= (-1 + \rho_2) H_2 \cos i \cdot \sin\theta - (1 + \rho_1) H_1 \cos\theta \\ H_y &= (-1 + \rho_2) H_2 \cos i \cdot \cos\theta + (1 + \rho_1) H_1 \sin\theta \\ E_z &= (1 + \rho_1) E_1 \sin i \end{aligned}\right\} \quad \cdots\cdots\cdots\cdots\cdots\cdots (2)$$

We discuss the following two cases.

I ; dry ground, $\kappa = 4$, $\sigma = 5 \times 10^{-5}$ υ/m

II; wet ground, $\kappa = 8$, $\sigma = 5 \times 10^{-3}$ υ/m

We will firstly investigate the errors due to low ground conductivity which are contained within the physical properties obtained with the CRT method.

If $E_z = 0$, equation (2) gives that $H_x/H_y = \tan\theta$ for the cutting axis of a half ellipse. Thus, the arriving direction θ contains no error. When H_x and H_y are rotated counter-clockwise by angle θ, the new axes are written as $\overline{H}_x$ and $\overline{H}_y$.

$$\overline{H}_x = -(1 + \rho_1) \cdot H_1$$

$$\overline{H}_y = (-1 + \rho_2) \cdot H_2 \cos i$$

The errors within A_2/A_1 and ϕ can be discussed on $\overline{H}_x - \overline{H}_y$ figure shown in Fig. 24, if we investigate the K and $\Delta\phi$ values given by the following equations.

$$K = \frac{(c^2 + d^2)^{1/2}}{(a^2 + b^2)^{1/2}} = \frac{A_2 \cos i}{A_1} \left\{ \frac{1 - 2|\rho_2| \cdot \cos\Theta_2 + |\rho_2|^2}{1 + 2|\rho_1| \cdot \cos\Theta_1 + |\rho_1|^2} \right\}^{1/2}$$

If we define Δk as $\Delta k = K - k$, we get

$$\Delta k/K = 1 - \left\{ \frac{1 + 2|\rho_1| \cos\Theta_1 + |\rho_1|^2}{1 - 2|\rho_2| \cos\Theta_2 + |\rho_2|^2} \right\}^{1/2}$$

where,

$$a = -A_1 (1 + |\rho_1| \cos\Theta_1)$$

$$b = A_1 |\rho_1| \sin\Theta_1$$

$$c = A_2 \cos i \{-\cos\phi + |\rho_2| \cos(\phi - \Theta_2)\}$$

$$d = A_2 \cos i \{-\sin\phi + |\rho_2| \sin(\phi - \Theta_2)\}$$

And

$$\sin(\phi + \Delta\phi) = \frac{|ad - bc|}{(c^2 + d^2)^{1/2}} \Big/ (a^2 + b^2)^{1/2}$$

So,

$$\cos \Delta\phi = \frac{1 - |\rho_2| \cos\Theta_2 + |\rho_1| \cos\Theta_1 - |\rho_1||\rho_2| \cos(\Theta_2 - \Theta_1)}{(1 + 2|\rho_1| \cos\Theta_1 + |\rho_1|^2)^{1/2} (1 - 2|\rho_2| \cos\Theta_2 + |\rho_2|^2)^{1/2}}$$

$$\sin \Delta\phi = \frac{|\rho_2| \sin\Theta_2 + |\rho_1| \sin\Theta_1 + |\rho_1||\rho_2| \sin(\Theta_2 - \Theta_1)}{(1 + 2|\rho_1| \cos\Theta_1 + |\rho_1|^2)^{1/2} (1 - 2|\rho_2| \cos\Theta_2 + |\rho_2|^2)^{1/2}}$$

Assuming that the reflecting surfaces are dry and wet grounds, $\Delta k/K$ and $\Delta\phi$ are calculated as shown in Fig. 25. It is found in the figure that $\Delta k/K$ and $\Delta\phi$ for the wet ground are negligibly small in VLF range unless an incident angle approaches too near to right angle and that those for the dry ground are roughly negligible if the frequency is in VLF range and the incident angle is not so large.

On the other hand, we can get the value of $\{(m'/p') K \sin\theta \sin(\phi + \Delta\phi)\}$ on Fig. 24 through the same process as we took for the perfectly conductive surface and it can be easily shown that the value is equal to sin i. Therefore, the incident angle i contains no error.

Next, we will check the error within the polarization obtained with the polarimeter and pen-oscillograph system. For simplicitie's sake, we assume that the received signal is right-handed circularly polarized. So, the polarization for perfect ground conductivity is

$$C_p = (1 + \cos i)/(1 - \cos i)$$

and the polarization for low ground conductivity is

$$C_L = [\cos^2 i\,(|\rho_2|^2 - 2|\rho_2|\cos\Theta_2 + 1) + (|\rho_1|^2 + 2|\rho_1|\cos\Theta_1 + 1) - 2\cos i \cdot$$
$$\{|\rho_1||\rho_2|\cos(\Theta_1 - \Theta_2) - |\rho_1|\cos\Theta_1 + |\rho_2|\cos\Theta_2 - 1\}]/$$
$$[\cos^2 i\,(|\rho_2|^2 - 2|\rho_2|\cos\Theta_2 + 1) + (|\rho_1|^2 + 2|\rho_1|\cos\Theta_1 + 1) + 2\cos i \cdot$$
$$\{|\rho_1||\rho_2|\cos(\Theta_1 - \Theta_2) - |\rho_1|\cos\Theta_1 + |\rho_2|\cos\Theta_2 - 1\}]$$

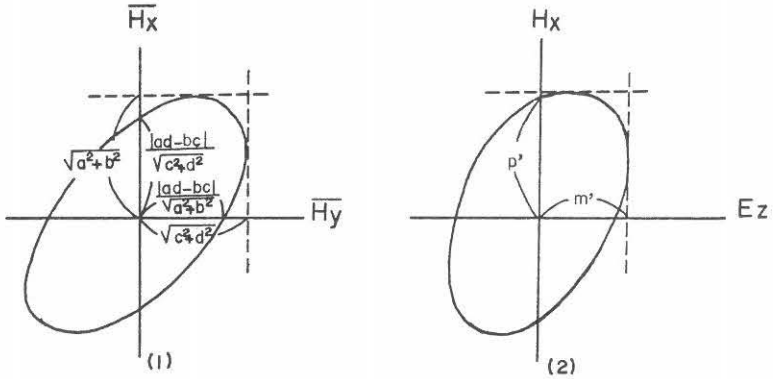

Fig. 24. (1) $\overline{H}_x - \overline{H}_y$ figure when the conductivity is low.
(2) $H_x - E_z$ figure when the conductivity is low.

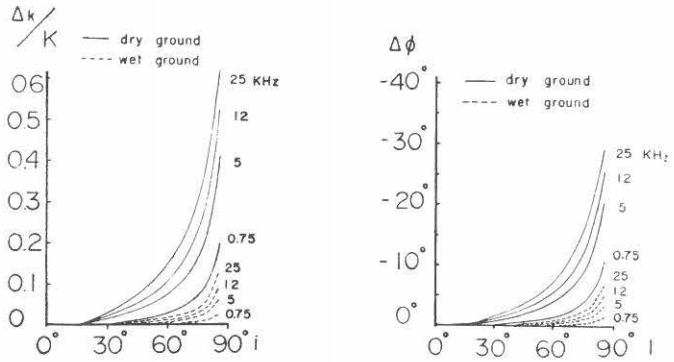

Fig. 25.

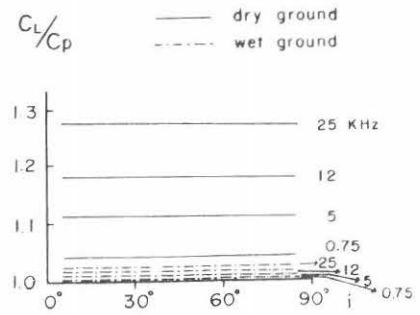

Fig. 26. The ratio of the polarization C_L for low ground conductivity to the polarization C_P for perfectly conductive ground on the assumption that the received signal is right-handed circularly polarized.

C_L/C_p is calculated and shown in Fig. 26. Fig. 26 shows that the errors within the polarizations are negligible in VLF range for the wet ground and even for the dry ground.

In conculusion, we may neglect the errors due to low ground conductivity within the polarization ratio A_2/A_1, the phase difference ϕ and the polarization R/L of VLF hiss, in general.

References

Ellis G. R. ; Low Frequency Electromagnetic Radiation associated with magnetic disturbances, P. S. S. 1, 253, 1959.

Ellis G. R. ; Directional observations of 5 kc/s Radiation from the Earth's Outer Atmosphere, J. G. R. 65, 839, 1960.

Harang L. & R. Larsen ; Radio Wave Emissions in the VLF band observed near the auroral zone - I Occurrence of emissions during disturbances, J. A. T. P. 27, 481, 1965.

Harang L. & K. N. Hauge ; Radio Wave Emissions in the VLF band observed near the auroral zone - II physical properties of the emissions, J. A. T. P. 27, 499, 1965.

Holt O. & A. Omholt ; Auroral luminosity and absorption of cosmic radio noise, J. A. T. P. 24, 467. 1962.

Iwai A. ; Study of the observational method of Atmospherics and Whistlers, in japanese Doctoral Thesis Nagoya Univ. 1962.

Iwai A. et al. ; The Observation of VLF emissions at Moshiri, Proc. Res. Inst. Atmospherics Nagoya Univ. **11**, 29, 1964.

Iwai A. & Y. Tanaka ; Measurement of polarization, incident angle and direction of VLF Emissions - (I), Proc. Res Inst. Atmospherics Nagoya Univ. **15**, 1, 1968.

Nishino M. & Y. Tanaka ; Polarization and arriving direction of VLF emissions at Syowa Base, Proc. Res. Inst. Atmospherics Nagoya Univ. **16**, 81, 1969.

Tanaka Y. et al. ; VLF hiss at Syowa Station, Antarctica, Proc. Res. Inst. Atmospherics Nagoya Univ. **17**, 43 1970.

Vershinin E. F. ; About the intensity of the hiss near inner boundary of the plasmapause and about the bursts of hiss with drifting frequency, Ann. Geophys. **26**, 703, 1970.